BBA - Biomembranes 1863 (2021) 183467

Contents lists available at ScienceDirect

BBA - Biomembranes

journal homepage: www.elsevier.com/locate/bbamem

Asymmetric bilayers mimicking membrane *rafts* prepared by lipid exchange: Nanoscale characterization using AFM-Force spectroscopy

Romina F. Vázquez[a,b,*], Erasmo Ovalle-García[c], Armando Antillón[c], Iván Ortega-Blake[c], Laura S. Bakás[d], Carlos Muñoz-Garay[c], Sabina M. Maté[a,*]

[a] Instituto de Investigaciones Bioquímicas de La Plata (INIBIOLP), CCT- La Plata, CONICET, Facultad de Ciencias Médicas, Universidad Nacional de La Plata, 60 y 120, 1900 La Plata, Argentina
[b] Departamento de Química, Facultad de Ciencias Exactas, Universidad Nacional de La Plata, 47 y 115, 1900 La Plata, Argentina
[c] Instituto de Ciencias Físicas, Universidad Nacional Autónoma de México, Av. Universidad 2001, Col. Chamilpa, 62210 Cuernavaca, México
[d] Centro de Investigación en Proteínas Vegetales (CIProVe), Departamento de Ciencias Biológicas, Facultad de Ciencias Exactas, Universidad Nacional de La Plata, 47 y 115, 1900 La Plata, Argentina

ARTICLE INFO

Keywords:
Lipid asymmetry
Sphingomyelin
Lipid domains
Supported lipid bilayers
Atomic force microscopy
Force spectroscopy

ABSTRACT

Sphingolipids-enriched *rafts* domains are proposed to occur in plasma membranes and to mediate important cellular functions. Notwithstanding, the asymmetric transbilayer distribution of phospholipids that exists in the membrane confers the two leaflets different potentials to form lateral domains as next to no sphingolipids are present in the inner leaflet. How the physical properties of one leaflet can influence the properties of the other and its importance on signal transduction across the membrane are questions still unresolved. In this work, we combined AFM imaging and Force spectroscopy measurements to assess domain formation and to study the nanomechanical properties of asymmetric supported lipid bilayers (SLBs) mimicking membrane *rafts*. Asymmetric SLBs were formed by incorporating N-palmitoyl-sphingomyelin (16:0SM) into the outer leaflet of preformed 1,2-Dioleoyl-sn-glycero-3-phosphocholine (DOPC)/Cholesterol SLBs through methyl-β-cyclodextrin–mediated lipid exchange. Lipid domains were detected after incorporation of 16:0SM though their phase state varied from gel to liquid ordered (*Lo*) phase if the procedure was performed at 24 or 37 °C, respectively. When comparing symmetric and asymmetric *Lo* domains, differences in size and morphology were observed, with asymmetric domains being smaller and more interconnected. Both types of *Lo* domains showed similar mechanical stability in terms of rupture forces and Young's moduli. Notably, force curves in asymmetric domains presented two rupture events that could be attributed to the sequential rupture of a liquid disordered (*Ld*) and a *Lo* phase. Interleaflet coupling in asymmetric *Lo* domains could also be inferred from those measurements. The experimental approach outlined here would significantly enhance the applicability of membrane models.

1. Introduction

Plasma membranes of cells present an asymmetric distribution of their phospholipid components between the two membrane leaflets [1]. Most phosphatidylcholine (PC) and sphingomyelin (SM) are present in the outer leaflet, whereas phosphatidylserine, phosphatidylethanolamine, and phosphatidylinositol are located in the inner leaflet. Cells actively maintain this asymmetry by investing high amounts of energy through ATP-dependent mechanisms [2]. The loss of this particular distribution triggers cellular processes like apoptosis and platelet activation and has also been related to pathological conditions like inflammation, neurodegenerative processes, and cancer [3–6].

Besides transbilayer lipid asymmetry, lateral heterogeneities also exist in plasma membranes, *i.e.*, organized structures occur in the plane of the membrane that differ in lipid and/or protein composition from the surrounding membrane, and lipid-lipid interactions are of

Abbreviations: SLs, sphingolipids; PC, phosphatidylcholine; SM, sphingomyelin; DOPC, 1,2-dioleoyl-sn-glycero-3-phosphocholine; 16:0SM, N-palmitoyl-sphingomyelin; Chol, cholesterol; bSM, brain sphingomyelin; MβCD, methyl-β-cyclodextrin; *Lo*, liquid ordered; *Ld*, liquid disordered; SLBs, supported lipid bilayers; AFM, atomic force microscopy; FS, Force spectroscopy; FvsD, Force *vs.* distance; Fb, breakthrough force; FvsS, Force *vs.* Tip-sample separation; *d*, rupture depth; MLVs, multilamellar vesicles; SUVs, small unilamellar vesicles; LUVs, large unilamellar vesicles; GUVs, giant unilamellar vesicles

* Corresponding authors at: INIBIOLP, CCT- La Plata, CONICET, Facultad de Ciencias Médicas, Universidad Nacional de La Plata, 60 y 120, 1900 La Plata, Argentina.
E-mail addresses: rvazquez@quimica.unlp.edu.ar (R.F. Vázquez), smate@med.unlp.edu.ar (S.M. Maté).

https://doi.org/10.1016/j.bbamem.2020.183467
Received 27 April 2020; Received in revised form 7 August 2020; Accepted 24 August 2020
Available online 29 August 2020
0005-2736/

fundamental importance for the emergence of such domains [7,8]. Among these specialized structures, the so-called *lipid rafts* have been proposed to act as key platforms for cellular functions like signal transduction, trafficking, and binding of biomolecules [9–12]. According to the raft hypothesis, the interaction between sphingolipids (SLs) and cholesterol (Chol) leads to the formation of segregated Chol- and SLs-enriched domains in the membrane where proteins can be selectively included or excluded [9,10,13]. It is worth mentioning that no direct evidence for lipid *rafts* actually occurring in biological membranes has been obtained yet—probably due to its proposed dynamic characteristics and small size [14,15]. An important move in this direction has been the work by Katsaras and colleagues who detected nanoscopic lateral membrane structures (< 40 nm) in living bacterial cells by neutron scattering, supporting the notion that nanoscopic lipid assemblies are an integral feature of biological membranes [16]. Moon and co-workers have also observed the formation of low-polarity nanoscale heterogeneities in live-cell membranes upon cholera-toxin treatment using spectrally resolved super-resolution microscopy with polarity-sensing molecules. Nevertheless, those nanodomains were only observed in treated cells suggesting that *raft*-like domains may be absent in native cells [17].

Studies in model membranes have shown that in lipid mixtures comprising certain SLs plus Chol and a low-melting PC, SLs and Chol indeed segregate forming domains which are in a liquid-ordered (*Lo*) phase—an intermediate physical state between the highly mobile liquid-disordered (*Ld*) and the solid-ordered (gel) phase [13,18–21].

Notwithstanding, most of the information concerning phase segregation and domain formation has come from studies using symmetric model membranes and the impact of lipid asymmetry on membrane properties has been disregarded. The distinctive lipid compositions of the inner and outer leaflets give them different potentials to form lateral domains. As next to no SLs are present in the inner leaflet, its potential to form ordered domains is expected to be lower than that of the outer leaflet. Consequently, the formation of *raft* domains would be limited to the external leaflet of the plasma membrane giving rise to asymmetric assemblies with an opposing leaflet formed by inner leaflet lipids which are not prone to form ordered domains by themselves [22]. The presence of Chol, though, in combination with interleaflet coupling can likely facilitate lateral structure in the inner leaflet as well [23]. Transbilayer coupling can, therefore, modulate the cell membrane organization and play a relevant role in signal transduction processes across the membrane where *raft*-like domains are proposed to participate.

In the last years, new methodologies for preparing asymmetric model membranes have been developed and improved [24–30]. Among them, the exchange of outer membrane lipids catalyzed by cyclodextrins has been successfully applied in the design of asymmetric small, large, and giant unilamellar vesicles (SUVs, LUVs, and GUVs) [28,31,32]. These model membranes maintained a stable transbilayer lipid asymmetry for several hours allowing the study of the physical properties of each hemilayer through different biophysical approaches including small-angle neutron scattering (SANS) [33], and fluorescence techniques like Förster resonance energy transfer (FRET) [34], fluorescence correlation spectroscopy (FCS) [32,35], and fluorescence microscopy [23], among others. Interleaflet coupling was found to be highly dependent on the lipid composition of each hemilayer. In some cases, one leaflet can influence the physical properties of the other with consequences in the formation of membrane domains, *i.e.*, in certain lipid mixtures, the presence of ordered domains in one leaflet can induce ordered domains in the opposite leaflet while in others, the formation of ordered domains can be prevented by a disordered phase in the opposing leaflet. In other cases, neither leaflet dominates and an intermediate order is found or no coupling at all occurs and each leaflet retains its own physical properties [23,33–37].

Recently, Visco et al. applied the Methyl-β-cyclodextrin (MβCD)–mediated lipid exchange method to prepare supported lipid bilayers (SLBs) with asymmetric lipid composition [38]. By incorporating brain SM (bSM) into the outer leaflet of DOPC supported bilayers, asymmetric membranes were obtained that maintained their lipid asymmetry for several hours. Interestingly, when bSM and Chol were sequentially incorporated into DOPC bilayers, no phase segregation was observed when inspected by fluorescence microscopy if no bSM was present in the inner leaflet.

In this study, we extend the analysis of the physical properties of asymmetric ternary SLBs prepared by MβCD-mediated lipid exchange to the nanoscale resulting in the first detailed characterization of asymmetric bilayers obtained by lipid substitution that mimic membrane *rafts*. To this end, we performed AFM imaging to study the topographic properties and phase behavior of lipid bilayers after the incorporation of N-palmitoyl sphingomyelin (16:0SM) into the outer leaflet of DOPC/Chol supported bilayers, and compared them with those of symmetric DOPC/16:0SM/Chol SLBs, a segregated two-phase system that has been thoroughly characterized by our group and which is relevant as a mammalian membrane model [39–42]. Force spectroscopic (FS) measurements were used as a complement to AFM topography to gain insights into the nanomechanical properties of the asymmetric bilayers [43,44]. These combined techniques provide nanometer/nanonewton resolution allowing the study of phase segregation and the physical properties of the bilayers avoiding the use of fluorescent probes or labeled lipid analogs. Measurements revealed phase segregation after incorporation of 16:0SM to DOPC/Chol supported bilayers, although differences in domains morphology, size, apparent height, and mechanical properties were found when compared to the symmetric DOPC/16:0SM/Chol ternary system depending on the temperature at which the lipid exchange process occurred. These results are discussed in terms of the mechanism of domain formation when using this methodology. Finally, interleaflet coupling in *Lo* domains is analyzed based on Force *vs.* Distance curves data.

2. Experimental section

2.1. Materials

1,2-Dioleoyl-sn-glycero-3-phosphocholine (DOPC), N-palmitoyl-D-erythro-sphingosyl phosphorylcholine (16:0SM), and cholesterol (Chol) were purchased from Avanti Polar Lipids (Birmingham, AL, USA) and used without further purification. Methyl-β-cyclodextrin (MβCD), N-(2-Hydroxyethyl)piperazine-N′-(2-ethanesulfonic acid) (HEPES), NaCl, $CaCl_2$, and other reagents, all analytical-grade, were acquired from Sigma–Aldrich (St. Louis, MO, USA). HPLC-grade chloroform and methanol were purchased from Merck (Darmstadt, Germany). Muscovite mica grade V-1 was purchased from SPI supplies (West Chester, PA, USA). All the solutions were prepared in ultrapure MilliQ water (resistivity of 18.2 MΩ.cm at 23 °C; Merck Millipore, Burlington, WI, USA).

2.2. Vesicles preparation

Multilamellar vesicles (MLVs) were prepared by mixing the appropriate amounts of synthetic pure lipids (DOPC, Chol, 16:0SM (2:1:1 mole ratio)) dissolved in chloroform/methanol (2:1, v/v). The samples were dried by evaporating the solvent under a stream of nitrogen and then placed under vacuum overnight to further remove the solvents. The dried lipid films were hydrated in HEPES-buffered saline (HBS Buffer: 20 mM HEPES, 150 mM NaCl, pH 7.4) at 65 °C, helping dispersion by stirring, until complete lipid detachment (the final lipid concentration was 150 μM). For obtaining small unilamellar vesicles (SUVs), MLVs were introduced in a Branson 1200 bath sonicator (Branson Ultrasonics Corp., Dansbury, CT, USA) and kept at 65 °C for 1 h. For vesicles containing only DOPC or DOPC/Chol (3:1 mole ratio), the same protocol was used but performed at 40 °C.

2.3. Preparation of MβCD-16:0SM complexes

MLVs of 16:0SM were prepared as described previously and mixed with a MβCD stock solution prepared in HBS buffer. The final concentrations in the mixture were 20 and 5 mM, respectively. After incubating for 3 h at 70 °C with continuous shaking, the mixture was centrifuged at 54,000*g* for 20 min at 4 °C. The supernatant containing the MβCD−16:0SM complexes was then separated, filtered through 0.22 μm filters and stored at −20 °C until used.

2.4. Formation of supported lipid bilayers (SLBs)

For AFM imaging and force spectroscopic measurements, SLBs were prepared on mica substrates using the vesicle adsorption technique [45]. Freshly cleaved mica previously mounted onto a liquid cell was pretreated with 120 μL of HBS Buffer containing 3 mM $CaCl_2$ for 15 min at 55 °C. Sonicated vesicles (65 μL, 150 μM) were then added on top of the mica and left to adsorb and extend for 30 min with the sample temperature maintained at 55 °C for DOPC/16:0SM/Chol mixtures or at 40 °C for DOPC and DOPC/Chol SLBs. The samples were left for further 60 min to equilibrate at room temperature after which the nonadsorbed vesicles were removed by washing 10 times with HBS buffer. A small amount of buffer was always left on top of the substrate to maintain hydration of the supported bilayers at all times. The liquid cell was set to 24 °C and the lipid bilayers were left to equilibrate for another 30 min before measurements.

2.5. Formation of asymmetric SLBs through MβCD-mediated lipid exchange

To prepare asymmetric DOPC/16:0SM/Chol bilayers, DOPC/Chol (3:1 mole ratio) supported bilayers were initially obtained. SLBs were inspected through AFM imaging to verify the formation of a completely covered defect-free surface, and FS measurements were performed on the binary system. To incorporate 16:0SM into the outer hemilayer, 60 μL of MβCD−16:0SM complexes (5 mM) were added to the DOPC/Chol SLBs and incubated at 24 °C or 37 °C for 30 min. SLBs were then delicately washed 10 times with HBS buffer and left to equilibrate at 24 °C.

2.6. AFM imaging

The measurements were performed using an XE-Bio AFM (Park Systems Corp., Korea) at 24 °C. Silicon nitride cantilevers (MSNL-10, Bruker Nano Inc.) with nominal spring constants of 0.01–0.1 N/m and nominal tip radius of 2 nm were used. Images were collected in contact mode at 512 × 512-pixel resolution at a scanning rate between 1 and 1.5 Hz maintaining the minimum possible force and were analyzed using the XEI Image Processing program from Park Systems.

For calculating the average height of the domains, at least 3 independent samples (n) were analyzed. 10–20 domains heights (N) were measured for each sample from three different images by tracing different line profiles. Average heights are reported as mean ± SD (N = 125, n = 6, for symmetric SLBs; N = 93, n = 5 and N = 40, n = 3, for asymmetric SLBs prepared at 37 °C and 24 °C, respectively).

Roughness measurements were performed by surface analysis on 2 μm^2 areas at different locations of three AFM images (10 × 10 μm^2) taken from each sample, using three different samples for DOPC/Chol (N = 52) and two independent samples for DOPC (N = 33) SLBs. Mean values ± SD are reported.

2.7. Force spectroscopy measurements

For FS measurements on SLBs, the optical lever sensitivity for each silicon nitride MSNL-10 cantilever (Bruker, Billerica, MA, USA) was calibrated acquiring a force curve in a lipid-free mica substrate. The spring constant of each cantilever was independently determined using the thermal noise method routine included in the XEI software. SLBs were first imaged and then Force *vs.* distance (F*vs*D) curves were acquired at 1 μm/s and 1 Hz. The curves were taken in a 2D grid of 256 individual curves over representative areas of the bilayer (1 μm × 1 μm or 3 μm × 3 μm). Approach and retraction curves were composed of 1024 (distance, force) ordered-pairs each. F*vs*D curves were analyzed to obtain the Breakthrough force (Fb) values using a home-made Matlab (MathWorks) routine adapted from Li et al. [46]. Matlab was also used to generate the corresponding Fb histogram plots. The F*vs*D curves were transformed to Force *vs.* Tip-sample Separation (F*vs*S) curves by calculating Tip-sample separation as $S = D + (F / k_c)$; where k_c is the calibrated cantilever spring constant. In this scheme, the signal of the rupture process is enhanced. By taking the derivative of the Force, the highest peak yields the rupture force while the width yields the penetration depth into the membrane (*d*). The bilayers Young's modulus was calculated by fitting the indentation region of F*vs*S curves using the classical Hertz contact model [47].

Distributions were generated from at least three independent sample preparations measured with at least three different tips (each sample prepared independently on a different day). Values were obtained from Gaussian fits of the corresponding distributions using Origin 8.5 software (OriginLab Corp, Northampton, MA, USA) and are presented as mean ± SD. Analysis of variance was performed using SigmaPlot 11.0 (Systat software, San Jose, CA, USA). Differences were significant for $p < 0.05$.

3. Results and discussion

3.1. Symmetric DOPC/16:0SM/Chol SLBs

The symmetric ternary mixture DOPC/SM/Chol has been widely studied as a relevant mammalian membrane model [20,39,48–50]. As mentioned before, the preferential interaction between SM and Chol in these systems results in the formation of SM/Chol-enriched *Lo* domains segregated from a DOPC-enriched *Ld* phase. The *Lo* phase is characterized by a lipid packing similar to the gel state, with ordered and relatively extended acyl chains, that nonetheless also exhibits high rotational and lateral diffusion rates similar to those of the *Ld* phase [51]. This difference in lipid packing produces Ångstrom- to nanometer-scale height differences between the lipid phases that can be evidenced by AFM microscopy [52].

In order to compare the structural and physical properties of asymmetric bilayers obtained by MβCD-mediated lipid exchange with their symmetric counterparts, we first characterized the DOPC/16:0SM/Chol (2:1:1 mole ratio) SLBs obtained by the conventional vesicle fusion method with the same experimental conditions as for the asymmetric membranes. Phase segregation was clearly observed in AFM images of DOPC/16:0SM/Chol SLBs with well-defined bright *Lo* domains embedded in a continuous darker *Ld* phase (Fig. 1, Panel A). The height difference between the *Lo* domains and the *Ld* phase was 0.68 ± 0.06 nm (line profile in Fig. 1, Panel A) which is in agreement with previous reports [39,40,48].

FS measurements were performed on DOPC/16:0SM/Chol SLBs to study the nanomechanical properties of the lipid phases. Force curves were obtained by applying a constantly increasing force with the AFM cantilever tip on the SLBs. From these curves, the breakthrough force (Fb) was obtained which corresponds to the maximum force that the bilayer is able to withstand before rupture. This force represents a direct measurement of the membrane mechanical stability at the nanometer scale which is highly related to the intermolecular interactions between the lipid molecules. Two main distributions of Fb were observed centered at 4.2 ± 2.0 nN and 12.0 ± 2.7 nN (Fig. 1, Panel B), corresponding to *Ld* and *Lo* phases, respectively. These values were in close agreement with previous results on DOPC/16:0SM/Chol symmetric bilayers in which average values of 4.8 and 5.7 nN were reported for *Ld* phases and 12.3 and 11.3 nN for *Lo* phases [39,41]. Similar

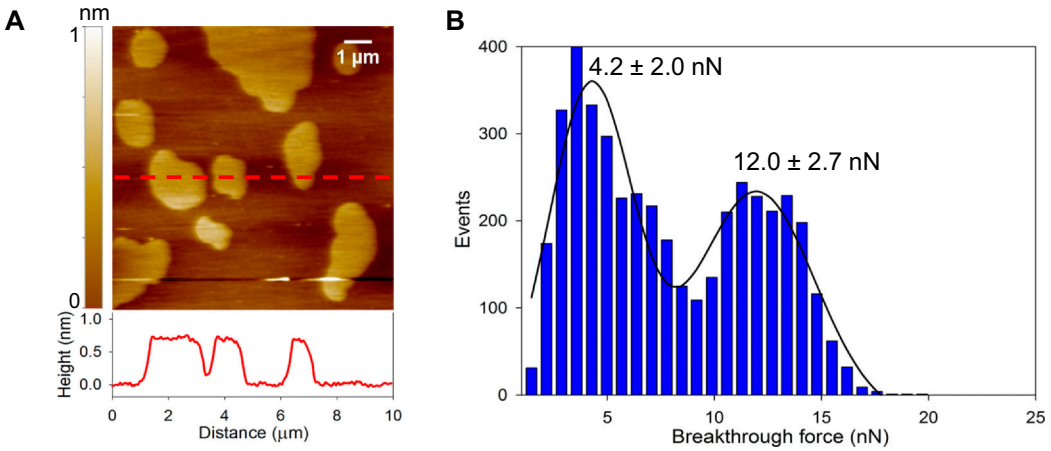

Fig. 1. AFM-FS measurements on DOPC/16:0SM/Chol SLBs. Panel A: AFM topographic image and height profile of a DOPC/16:0SM/Chol (2:1:1, molar ratio) supported bilayer obtained by vesicle fusion. The height profile was measured along the dashed red line depicted in the image. Panel B: Distribution of breakthrough force events in DOPC/16:0SM/Chol SLBs. The solid line corresponds to the Gaussian fitting of the data (N = 4300; from 8 independent tip/sample preparations). (For interpretation of the references to colour in this figure legend, the reader is referred to the web version of this article.)

results have also been reported for DOPC/18:0SM/Chol supported bilayers with average Fb values of 6.5 and 12.0 nN for the *Ld* and *Lo* phases, respectively [53]. The higher Fb values in the *Lo* phase reflect a more ordered packing between SM and Chol in that phase in comparison to the lipid packing in the DOPC-enriched *Ld* phase. It is worth mentioning that Fb values depend not only on the specific lipid composition but also on several variables like temperature, and buffer conditions (pH, ionic strength, presence of divalent cations), for instance, which affect the mechanical stability of the lipid bilayers [54–57]. Moreover, the chemical properties and geometry of the cantilever and its tip, the loading force, and approach velocity also influence the Fb values measured [20,58,59]. Therefore, the absolute values of rupture forces can only be compared when measurements are performed under very similar experimental conditions, even for the same lipid mixture.

3.2. DOPC/Chol SLBs as the starting point

To gain insights into the phase behavior of asymmetric membranes, the aim was to obtain ternary SLBs by incorporating 16:0SM into the outer leaflet of DOPC/Chol (3:1 mole ratio) bilayers. In order to limit the interaction of 16:0SM-MβCD complexes with the outer leaflet of the supported bilayer, DOPC/Chol SLBs were properly formed, free of bilayer defects and yielding a complete surface coverage as revealed by inspection of several areas of the mica. As an initial step, DOPC/Chol (3:1) SLBs were characterized, to confirm the correct formation of the bilayer and also to study the physical properties of the binary system before the incorporation of 16:0SM. Panel A in Fig. 2 shows a topographic image (shown as *inset*) and the Fb histogram obtained for DOPC/Chol (3:1) SLBs. Images showed smooth homogeneous surfaces with an average roughness (rms) of 0.055 ± 0.015 nm. Accordingly, a single distribution of Fb was measured at 7.5 ± 0.6 nN, in correspondence with a single lipid phase.

The Fb values of DOPC/Chol (3:1) bilayers were intermediate between those of the *Ld* and *Lo* phases of the ternary DOPC/16:0SM/Chol SLBs (*cf.* Fig. 1) and reflected a more ordered but still *Ld* phase. The interaction of Chol with DOPC is known to produce an ordering of the phospholipid hydrocarbon chains condensing the lipid and increasing its packing density giving a more compact bilayer structure [60,61]. In the ternary DOPC/16:0SM/Chol (2:1:1) system, Chol is assumed to be mostly concentrated in the *Lo* phase due to its interaction with SM and, consequently, the amount of Chol in that *Ld* phase is expected to be low, being DOPC its main lipid component. Considering this, we also performed measurements on neat DOPC SLBs to further study to which

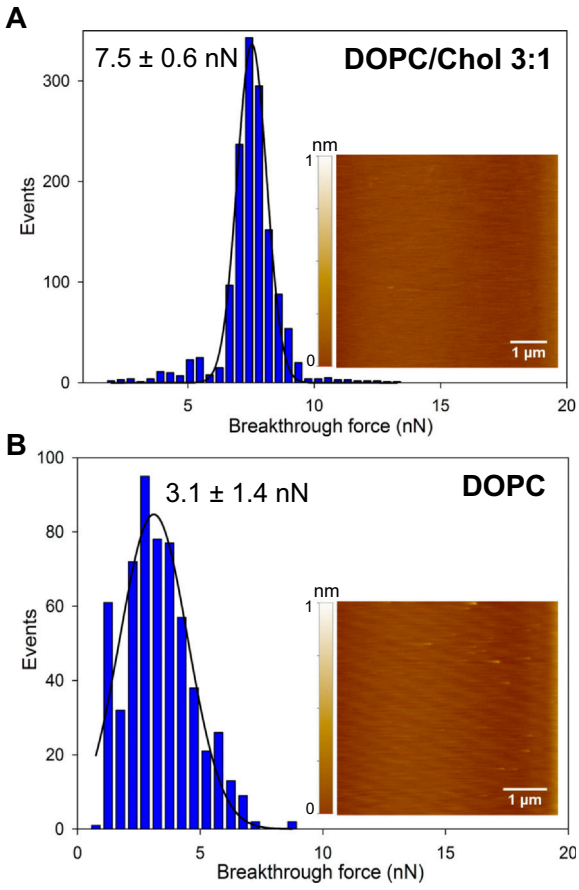

Fig. 2. AFM-FS measurements on DOPC/Chol and DOPC SLBs. AFM topographic images (*insets* in Panels A and B) and breakthrough force histograms of DOPC/Chol (3:1 mole ratio) (Panel A) and neat DOPC (Panel B) SLBs. The solid black lines in the histograms correspond to the Gaussian fitting of the data (N = 1450 from 3 independent tip/sample preparations for DOPC/Chol 3:1; N = 600 from 2 independent tip/sample preparations for DOPC). Measurements were performed at 24 ± 1 °C.

extent Chol could segregate from the *Ld* phase due to the incorporation of SM. DOPC formed uniform SLBs (*inset* in Fig. 2, Panel B) with rms values of 0.071 ± 0.040 nm. The bilayer rupture events occurred at average Fb of 3.1 ± 1.4 nN (Fig. 2, Panel B). These results are in good

agreement with data from other groups reporting average values in the range of 1.7–5 nN for DOPC [53,59,62,63]. The ordering effect of Chol on DOPC SLBs was therefore reflected in the higher values of Fb obtained for DOPC/Chol (3:1) SLBs (7.5 nN) than for neat DOPC bilayers (3.1 nN). This same behavior has previously been shown in FS studies performed by Redondo-Morata et al. in which an increment in Fb values from 10 nN to 17–20 nN was registered when Chol was included up to 40 mol% in DOPC SLBs [60]. Notice that those measurements were performed in the presence of Mg^{2+} that stabilizes lipid bilayers and, therefore, higher Fb values were measured in both, DOPC and DOPC/Chol SLBs.

The Fb values registered in DOPC SLBs (3.1 nN) were similar to those of the *Ld* phase (4.2 nN) in DOPC/16:0SM/Chol (2:1:1) bilayers, reinforcing the notion that DOPC is the main lipid component of that phase in the symmetric ternary systems.

3.3. MβCD-mediated incorporation of 16:0SM into the outer leaflet of DOPC/Chol SLBs

DOPC/Chol (3:1) SLBs were then incubated with 5 mM MβCD-16:0SM complexes at 24 °C or 37 °C for 30 min and left to equilibrate at 24 °C before AFM-FS measurements. When the incubation was performed at 24 °C, AFM images revealed the presence of segregated micrometer-sized domains protruding from a continuous phase (Fig. 3, Panel A), evidencing the incorporation of 16:0SM. Also, smaller inhomogeneities were observed in the continuous phase that could account for submicrometer-sized domains. Microdomains presented an average height of 1.2 ± 0.2 nm, higher than that registered for *Lo* domains in the DOPC/16:0SM/Chol symmetric system (~0.7 nm). Membrane defects were detected inside these micrometer domains that reflected a less fluid phase than the *Lo* phase of the symmetric bilayers. The height and morphology of microdomains resembled more to SM-enriched domains in gel state rather than to the *Lo* domains observed in the symmetric system (*cf.* Fig. 1) [64,65]. When analyzing the F*vs*D curves, a broad range of Fb values was observed (Fig. 3, Panel B). Notwithstanding, few rupture events could be registered inside the micrometer-sized domains at the loading forces applied, which did occur at domains boundaries. The lower Fb forces were centered at ~6 nN which corresponded to a *Ld* phase and the higher rupture forces were centered at ~19 nN, although forces up to 35 nN were detected.

Neat 16:0SM SLBs have been reported to yield Fb values of 36.8 ± 3.7 nN when measured at 22 °C, temperature at which they are expected to be in a gel phase (Tm ~42 °C) while in mixtures with Chol, Fb forces decreased, as reported for 16:0SM/Chol (7:3) mixtures with Fb values of 23.7 nN [39]. AFM-FS studies performed by Sullan et al. on symmetric DOPC/18:0SM/Chol SLBs showed that domains formed in lipid mixtures with 5% Chol were predominantly in the gel phase while those formed in bilayers with 10% Chol appeared as a mixture of gel and *Lo* phases. When Chol contents were between 10 and 15%, the SM/Chol-enriched domains also presented less fluid characteristics than

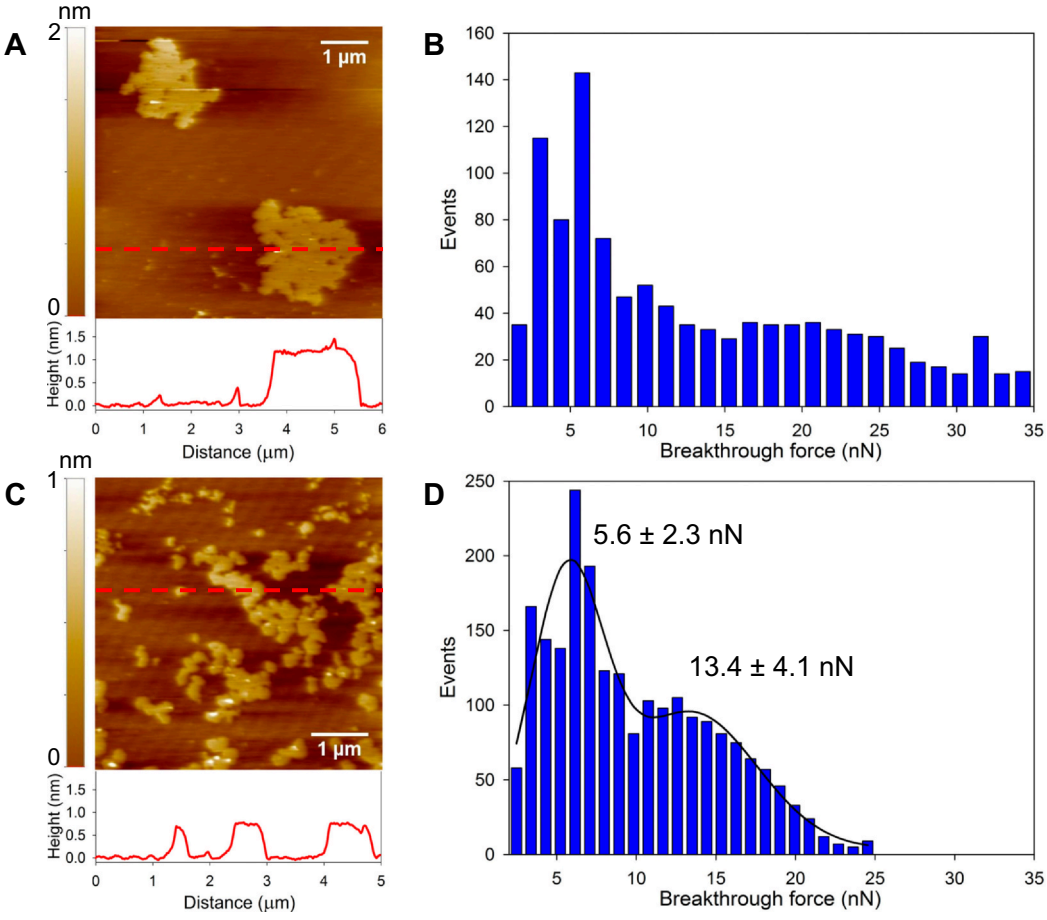

Fig. 3. AFM imaging and FS measurements on asymmetric membranes. Panels A and C: AFM topographic images and height profiles of DOPC/Chol SLBs after incubation with MβCD-16:0SM complexes at 24 °C (Panel A) or 37 °C (Panel C). Height profiles were measured along the dashed red lines depicted in the images. Panels B and D: Distribution of breakthrough forces measured in asymmetric ternary bilayers obtained at 24 °C (Panel B) or 37 °C (Panel D). The solid line in D corresponds to the Gaussian fitting of the data (Panel B: N = 1054, from 3 independent tip/sample preparations; Panel D: N = 2190 from 4 independent tip/sample preparations). All measurements were performed at 24 ± 1 °C. (For interpretation of the references to colour in this figure legend, the reader is referred to the web version of this article.)

those observed at 25% Chol which were in a *Lo* state [20]. Our results pointed to the formation of a mixture of gel and *Lo* 16:0SM-enriched domains over a wide range of SM/Chol compositions when 16:0SM was incorporated at 24 °C, being the richer in Chol the ones with the lower Fb. Accordingly, the Fb values of the *Ld* phase were lower than those of the initial DOPC/Chol (3:1) bilayer, indicating that the level of Chol decreased there due to its incorporation into the SM/Chol domains, although the partial removal of Chol from the SLBs by MβCD should not be discarded [66].

Next, we explored the results of lipid exchange when DOPC/Chol (3:1) SLBs were incubated with MβCD-16:0SM complexes at 37 °C to form asymmetric bilayers. Again, phase segregation was observed with light domains arising from a darker fluid phase (Fig. 3, Panel C). In this case, domains were smaller than those obtained at 24 °C with an average height of 0.72 ± 0.08 nm. The smaller height difference between the coexisting phases suggested that more Chol was incorporated in the SM/Chol domains, causing a loosening of SM lipid packing that led to a decrease in the height of the ordered phase. When the nanomechanical properties of the bilayers were measured, two main distributions of Fb were detected with average values of 5.6 ± 2.3 nN and 13.4 ± 4.1 nN which could be attributed to *Ld* and *Lo* phases, respectively (Fig. 3, Panel D). These Fb values were in accordance with those reported for *Ld* and *Lo* phases in the symmetric system (*Ld*: 4.2 nN; *Lo*: 12.0 nN, *cf.* Fig. 1, Panel B; [39] [41]), reflecting that the incorporation of 16:0SM by this procedure, when performed at 37 °C, favored SM/Chol interactions allowing the formation of *Lo* domains with similar mechanical stability as those observed in symmetric bilayers. Still, the *Ld* phase presented an average Fb lower than DOPC/Chol (3:1) SLBs (5.6 nN Ld_{asym} *vs.* 7.5 nN DOPC/Chol) but higher than neat DOPC bilayers (3.1 nN).

The Chol levels in SM/Chol-domains affect their morphology and nanomechanical properties. While round domains are observed at high Chol concentrations (15–30%) in PC/SM/Chol mixtures, at low Chol content (5–15%) small taller domains appear that tend to form close networks with other domains [20]. Accordingly, the Fb of domains decreases as the Chol content increases, consistent with the fluidizing effect of Chol on SM-enriched domains and its role in the formation of the *Lo* phase [18,20]. Considering our results, the segregated *Lo* domains that formed after incorporation of 16:0SM into the outer leaflet of DOPC/Chol SLBs at 37 °C must differ in SM/Chol ratio within a narrow range (being all in a *Lo* phase), resulting in a broader distribution of Fb values compared with the symmetric system (*cf.* Fig. 1). On average, domains seemed to have less Chol content than symmetric *Lo* domains and, therefore, higher height and Fb values. Also, the *Ld* phase accounted for higher Chol levels remaining in this phase compared to the *Ld* phase of symmetric systems, as reflected in the higher Fb measured (5.6 nN Ld_{asym} *vs.* 4.2 nN Ld_{sym}). The lower Fb values of the *Ld* phase in asymmetric SLBs (5.6 nN) in comparison with those of the initial DOPC/Chol SLBs (7.5 nN), indicated that Chol levels decreased in that phase after the incorporation of SM but it was still present to some extent since this value was higher than the one obtained for neat DOPC bilayers (3.1 nN). Therefore, as in the asymmetric SLBs prepared by incubation at 24 °C, the overall final levels of Chol in the bilayers seem not to have been drastically affected by MβCD extraction after 16:0SM was delivered at 37 °C, as inferred from the Fb values of the *Ld* and *Lo* phases.

In line with Fb results, asymmetric bilayers presented slightly higher Young's moduli in the *Lo* and *Ld* phases than their symmetric counterparts (Fig. 4). Average Young's modulus of 9.8 ± 6.6 MPa and 12.4 ± 4.6 MPa were calculated for symmetric (Panel A) and asymmetric (Panel B) *Lo* domains, respectively, indicating that asymmetric domains showed similar resistance against the elastic deformation induced by the tip in the indentation region than symmetric ones. Higher contents of SM with an increased lipid packing in the external leaflet of asymmetric domains may account for the small differences observed as were also reflected in their higher Fb values. It is worth mentioning,

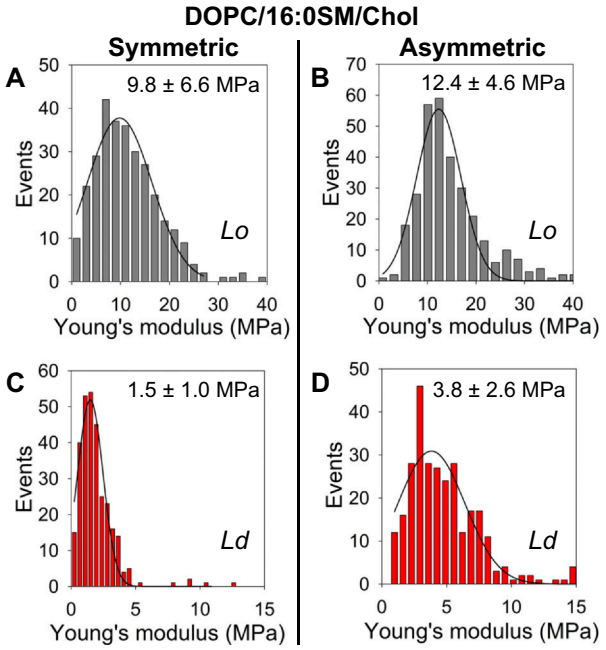

Fig. 4. Young's moduli of symmetric and asymmetric SLBs. Distributions of Young's modulus in DOPC/16:0SM/Chol SLBs prepared by vesicle fusion (symmetric, Panels A and C) and those prepared by MβCD-mediated SM exchange at 37 °C (asymmetric, Panels B and D). Gray histograms correspond to Liquid-ordered (*Lo*) phases (Panels A and B) and red histograms to Liquid-disordered (*Ld*) phases (Panels C and D). Solid lines represent the Gaussian fitting of the data. Values are reported as mean ± SD from 3 independent experiments measured with 3 different tips (each histogram contains N = 300). All measurements were performed at 24 ± 1 °C. (For interpretation of the references to colour in this figure legend, the reader is referred to the web version of this article.)

though, that different probes were used to get the force curves and small variations in the tip's radius could affect the absolute values of the calculated Young's moduli. On the other hand, in each system, the *Ld* phase showed lower Young's modulus than the *Lo* phase, as expected from its more fluid characteristics, with average values of 1.5 ± 1.0 MPa and 3.8 ± 2.6 MPa in symmetric (Panel C) and asymmetric (Panel D) SLBs, respectively. These results correlated with the relative higher Fb found in the *Ld* phase in asymmetric SLBs and likely resulted from a higher Chol content when compared to the symmetric system.

Sullan et al. have reported Young's moduli of ~80 MPa and ~140 MPa in *Ld* and *Lo* phases, respectively, in DOPC/SM/Chol SLBs [67]. The lower values obtained in our study may result from differences in the experimental conditions, most likely from the AFM tips used to acquire the force curves. Saavedra et al. have recently reported that small indenters—as the 2 nm tips used in this study—can produce lower Young's moduli than expected [59]. In their study, DOPC bilayers yielded Young's modulus of ~2 MPa when using 2 nm indenters—similar values than the ones reported here for the fluid *Ld* phases—and 34 MPa when 20 nm probes were used. Low values of Young's modulus have also been reported in fluid (4–6 MPa) and gel (10–20 MPa) phases in phase-separated SLBs containing milk SM measured with 2 nm indenters [47]. Therefore, the absolute values reported here should be considered with caution.

3.4. Transbilayer lipid asymmetry and interleaflet coupling in Lo domains

AFM images showed that partial replacement of lipids occurred after lipid exchange, inducing phase segregation while maintaining the integrity of the lipid bilayers. Notwithstanding, the average Fb value

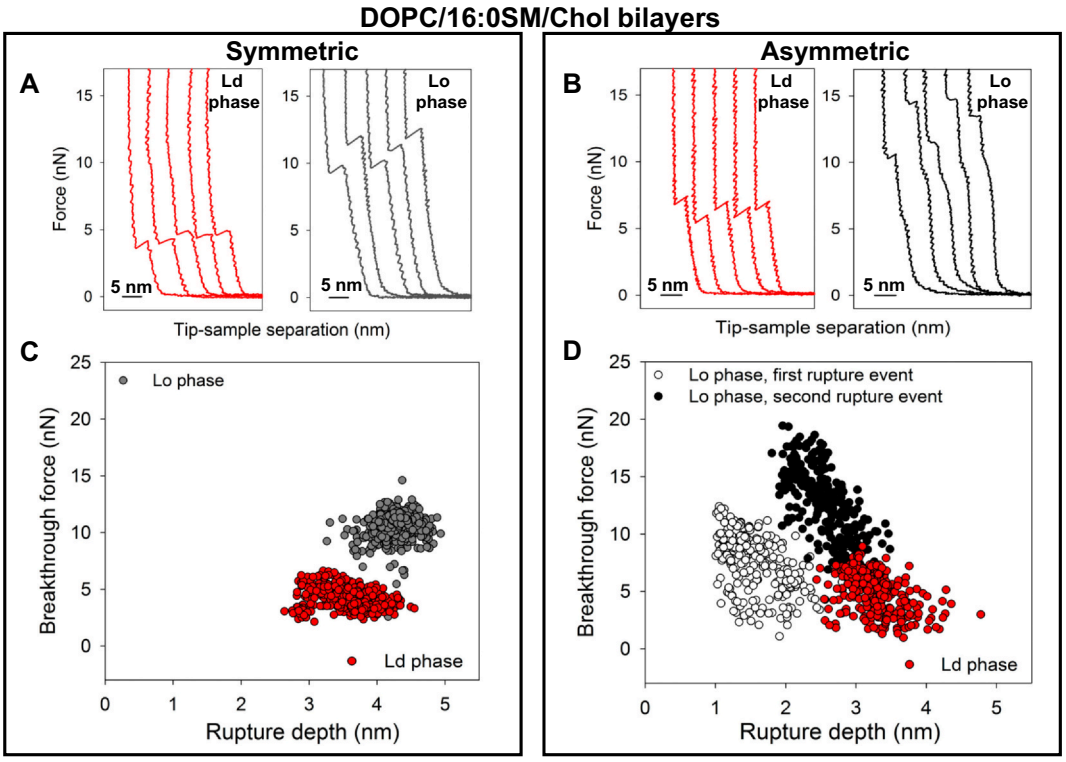

Fig. 5. Rupture events in symmetric and asymmetric DOPC/16:0SM/Chol SLBs. Force *vs.* Tip-sample separation (F*vs*S) curves were obtained from the corresponding F*vs*D curves. Panels A and B show typical F*vs*S curves obtained for the Liquid disordered (*Ld*) (left figures) and Liquid ordered (*Lo*) (right figures) phases in symmetric (A) and asymmetric (B) bilayers. From F*vs*S curves, the rupture depths (*d*) for the single breakthrough events observed in the *Ld* phases of both systems (symmetric and asymmetric) and in *Lo* domains of symmetric bilayers, as well as each consecutive rupture event observed in the *Lo* phase of asymmetric bilayers were calculated. Panels C and D show the Breakthrough force distributions as a function of the rupture depths obtained for each system. In both panels, red circles correspond to the rupture events registered in the *Ld* phase. Gray circles in Panel C correspond to the single rupture events registered in symmetric *Lo* domains while open circles and filled black circles in Panel D correspond to the first and second rupture events, respectively, registered in asymmetric *Lo* domains. F*vs*S curves from three independent samples measured with three different tips were analyzed for each system. N = 1120 for symmetric SLBs (600 *Ld*, 520 *Lo*); N = 800 for asymmetric SLBs (450 *Ld*, 350 *Lo*). All measurements were performed at 24 ± 1 °C. (For interpretation of the references to colour in this figure legend, the reader is referred to the web version of this article.)

corresponding to the *Lo* domains in the asymmetric SLBs was similar to that of the symmetric bilayers. The question that then arises is whether both leaflets were coupled or not and to what extent those domains were asymmetric in lipid composition.

To explore transbilayer lipid asymmetry and possible coupling of both leaflets in *Lo* domains, we then analyzed the F*vs*D curves. In FS measurements, the AFM tip approaches the bilayer at a constant speed. When the tip contacts the surface, an increasing force is observed in the F*vs*D curves; the bilayer is first indented as it is softer than the tip and finally, when the bilayer is no longer able to withstand the loading force, the tip breaks through the bilayer and reaches the substrate. Beyond this point, the cantilever starts to deflect since the substrate cannot be indented [46]. From F*vs*D curves, the corresponding Force *vs.* Tip-sample Separation (F*vs*S) curves can be obtained. Fig. 5 shows representative F*vs*S curves for *Ld* and *Lo* phases of symmetric DOPC/16:0SM/Chol SLBs prepared by vesicle fusion (Panel A) and asymmetric DOPC/16:0SM/Chol SLBs formed through MβCD-lipid exchange (Panel B). In symmetric SLBs, both, the *Ld* phase and *Lo* domains showed typical F*vs*S behavior, with one breakthrough event. From these curves, the rupture depth (*d*) could be estimated to be 3.7 ± 0.6 nm in the *Ld* phase (Fb = 4.4 ± 1.6 nN) and 4.3 ± 0.2 nm in the *Lo* phase (Fb = 11.0 ± 1.0 nN), which can be used as an estimation of the bilayer thickness at the rupture point. Rupture depths of 3.6 ± 0.2 nm have been reported for DOPC/Chol 9:1 bilayers which are in close agreement with our results for the *Ld* phase [61]. The higher rupture depth in the *Lo* phase reflects the more ordered packing of lipids rendering a thicker bilayer and is in accordance with the height differences between *Lo/Ld* phases observed in AFM images (*cf.* Fig. 1). It is worth to note that the rupture depths can only be considered as an estimation of the true bilayer thickness since they are measured at a point in which the bilayer is in compression and, therefore, those values are likely underestimated.

F*vs*S curves on the *Ld* phase of asymmetric bilayers also showed a single breakthrough step yielding an average rupture depth of 3.3 ± 0.7 nm at Fb values of 6.03 ± 0.9 nN, consistent with a *Ld* phase. A different behavior was observed in F*vs*S curves obtained in asymmetric *Lo* domains. Interestingly, two consecutive rupture events were detected, a clear breakthrough event that occurred at higher Fb values Fb_2 = 12.9 ± 3.6 nN (these higher Fb_2 values correspond to those included in the Fb histogram of Fig. 3 D) but also a less-defined breakthrough event appeared at 7.5 ± 2.4 nN (Fb_1). The rupture depths of these first events (d_1) were always lower than those of the second events (d_2), with average values of 1.6 ± 0.4 nm and 2.6 ± 0.3 nm for d_1 and d_2, respectively. Considered together, the two steps showed a total breakthrough of 4.1 ± 0.7 nm in asymmetric *Lo* domains, a value slightly smaller than the 4.3 nm observed in the symmetric ones. Panels C and D in Fig. 5 show the Fb *vs. d* distributions for symmetric and asymmetric bilayers, respectively.

Alessandrini et al. have studied the mechanical properties of single POPG and POPE bilayers prepared by different experimental procedures that enabled the obtention of SLBs with both leaflets in the same phase state (*i.e.*, symmetric SLBs) or in different phase states (*i.e.*, asymmetric SLBs). Measurements showed that, depending on the interleaflet coupling, the force curves on the bilayers can show one or two

rupture events: for uncoupled bilayers, the tip penetration occurred sequentially through the two leaflets giving rise to two penetration events, while in bilayers with coupled leaflets the jump of the AFM tip through the SLBs occurred in only one step [68]. A similar behavior comprising two breakthrough events was reported for DOPC/Chol SLBs with an asymmetric distribution of Chol between the two leaflets [61]. In those reports, the proximal leaflet, the one in close contact with the solid support, presented higher lipid density and, therefore, higher Fb values than the distal (external) leaflet. As a result, two well-defined rupture events were observed, with the second one occurring at higher Fb, consistent with these considerations. On the contrary, in our system, if 16:0SM was incorporated only in the outer leaflet, the *Lo* domains should be lying on top of a disordered DOPC-enriched hemilayer. In this situation, if the two leaflets are not strongly coupled, the force needed to rupture the *Lo* domains in the outer leaflet would be greater than that needed to break through the proximal leaflet. Considering this, it is tempting to propose that the first less-defined breakthrough step observed in F*vs*S curves of asymmetric *Lo* domains could be a result of the DOPC-enriched leaflet rupture not by means of tip penetration since *Lo* domains were still not pierced at those loading forces, but from the compression exerted by the whole tip-*Lo* phase system. When the tip reached the *Lo* domain surface, the high mechanical stability of the SM/Chol ordered phase could produce the compression of the less cohesive disordered DOPC-enriched hemilayer as the AFM tip pushed against the top of the *Lo* domains and the loading force increased. In the symmetric system, the proximal leaflet presents similar mechanical stability than the distal one and offers resistance to bilayer deformation and breakthrough, and the bilayer is then punctured as a whole when a force threshold is reached. In the asymmetric array, the presence of a less ordered phase with loosened lipid packing in the proximal leaflet offers a less effective mechanical barrier. As the DOPC-enriched hemilayer is then compressed, a force limit could be attained (~7.5 nN) at which this leaflet collapses but that it is still not high enough to break through the *Lo* domains. Only when the loading force reaches higher values (~13 nN), the tip jumps through the *Lo* domains and the second rupture event is observed. A schematic representation of these events is shown in Fig. 6.

In line with these considerations, the rupture depths of either event registered in asymmetric *Lo* domains were lower than that registered for symmetric domains (~4.3 nm) and could be attributed to a disordered hemilayer that collapsed first (~1.6 nm) at lower Fb forces, and a thicker ordered leaflet that was punctured in the second event (~2.6 nm) at the higher Fb. These depths cannot be unambiguously assigned, though, since the first rupture depth could correspond to only the partial breakdown of the proximal leaflet in which case the rupture depth of the second event would result from the combined rupture of the external *Lo* leaflet and the remaining proximal *Ld* leaflet compressed after the first rupture step. In any case, the *Ld* leaflet seemed to be ruptured first as inferred from the Fb values.

Domains formed in symmetric model membranes by conventional procedures are mostly aligned in both leaflets, implying the presence of strong interleaflet coupling [69]. In asymmetric model membranes, however, different levels of coupling have been reported depending on lipid composition, temperature, and curvature of the bilayer [33,34,70,71]. In our asymmetric system, if the two leaflets in the *Lo* domains were strongly coupled they would have been expected to break as a single unit as in the case of symmetric domains. The presence of the two rupture steps evidenced the absence of such a strong coupling, at least while under pressure—the pressure of the tip could also be inducing the uncoupling of both leaflets in which case FS measurements would result in an underestimation of the coupling phenomenon. Interestingly, the first rupture events occurred at ~7.5 nN, the mean value registered for DOPC/Chol (3:1) SLBs (*cf.* Fig. 2) while the second events occurred at ~13 nN, the values reported for SM/Chol-enriched *Lo* domains. If no coupling at all occurred between the two leaflets, the DOPC-enriched *Ld* phase in the proximal hemilayer of domains would have been expected to rupture at lower forces, such as those registered in the continuous *Ld* phase of this system (~6 nN). The actual higher Fb needed to rupture the proximal hemilayer could be indicative of coupling between the SM/Chol-enriched external leaflet and the DOPC-enriched proximal one rendering a *Ld* phase that differed from the overall *Ld* proximal leaflet, having probably more Chol content. That the mechanism proposed for the rupture of the proximal *Ld* leaflet in asymmetric *Lo/Ld* domains is different from that of the *Ld/Ld* array and that higher forces may be required to produce the proposed rupture by compression, should also be considered.

Topographic findings in our asymmetric system could also be indicative of transbilayer coupling. The height difference between the *Ld* and the *Lo* phase may be expected to be lower in asymmetric membranes where domains are formed only in the outer leaflet. Our results showed, however, that *Lo* domains formed after incubation with MβCD-SM at 37 °C, had similar average height as those observed in the symmetric system (0.72 nm *vs.* 0.68 nm, respectively) suggesting that the presence of SM-enriched *Lo* domains in the external leaflet could induce the ordering of the DOPC-enriched *Ld* proximal one producing a thicker bilayer than that expected from the sum of two independent *Lo/Ld* hemilayers.

Based on FS measurements, the coupling between leaflets in asymmetric *Lo* domains was neither strong nor too weak but likely occurred at an intermediate level. These findings agree with the observations made in asymmetric GUVs and LUVs in which the presence of ordered outer leaflets induced by the incorporation of SM increased the degree of inner-leaflet order [31,32]. Coupled leaflets in ordered domains have also been reported in asymmetric supported bilayers prepared by the Langmuir Blodgett-Vesicle fusion technique [36,70,72].

In summary, results presented here show that asymmetric SLBs with *raft*-like domains in the external leaflet can be obtained by incorporating 16:0SM into DOPC/Chol supported bilayers through MβCD-mediated lipid exchange and their topography, nanomechanical properties, and interleaflet coupling explored by AFM-FS.

Our results show that no SM is needed in the preformed SLBs to achieve phase segregation when 16:0SM is incorporated through 16:0SM − MβCD complexes. A similar procedure was applied by Visco et al. to prepare asymmetric SLBs [38]. In that study, the authors found that basal levels of SM were needed in the proximal leaflet to detect phase segregation when brain SM and Chol were introduced in the upper leaflet of DOPC bilayers. These discrepancies could result from the different acyl chain composition of the SMs that were used in each study, a factor that crucially affects phase segregation and domain size [73]. Brain extracts of SM have mainly 18:0SM (50%) but also a high proportion of unsaturated acyl chains (21% of nervonoyl-SM, 24:1-SM) and, both, unsaturation and N-acyl chain length affect lipid-lipid interactions and phase behavior in PC/SM/Chol mixtures [39,74–77]. 24:1-SM, in particular, can eventually prevent phase segregation in these ternary systems [39,42].

The phase state of the segregated domains obtained in our study varied from a mixture of gel/*Lo* to mainly *Lo* domains if 16:0SM was introduced into the preformed SLBs at 24 °C or 37 °C, respectively. Even when bilayers were always equilibrated at 24 °C before inspection, AFM-FS measurements revealed that the thermal history of the sample affects the morphology and physical properties of the resulting domains. The incorporation of 16:0SM in a more fluid bilayer (at higher T) favored its interaction with Chol allowing the formation of *Lo* domains, the physical phase state proposed for membrane *rafts*. One thing to take into consideration is the mechanism of domain formation when using the MβCD-mediated lipid exchange method. In this procedure, SM is incorporated from an exogenous source to preformed SLBs carried in a water-soluble MβCD-lipid complex. The dynamics of domain formation in these conditions must certainly be different from that occurring in symmetric bilayers prepared by conventional methods, and lipid organization can drastically depend on how the lipid composition is locally generated [78]. Domain structure is highly dependent on lipid

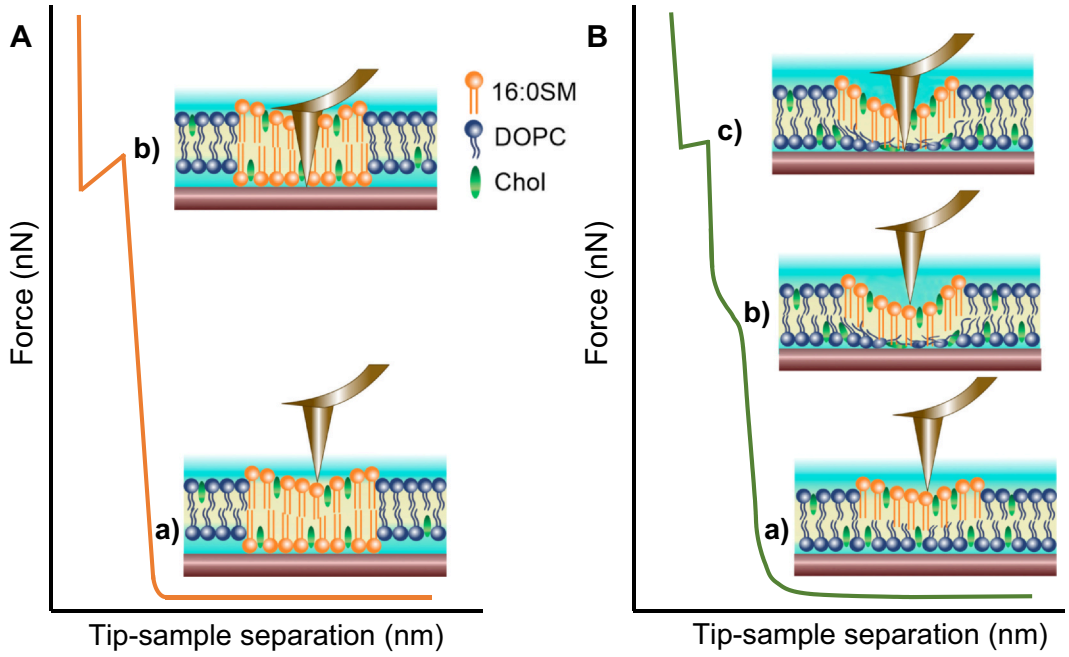

Fig. 6. Schematic representation of the rupture events in symmetric and asymmetric Lo domains. Typical Force *vs.* Tip-sample separation (F*vs*S) curves for symmetric (Panel A) and asymmetric (Panel B) *Lo* domains are presented. In these curves, the AFM tip approaches the bilayer at a constant speed. In symmetric *Lo* domains (Panel A) the two domain leaflets have similar mechanical stability. Once the tip contacts the surface, the loading force increases, and the bilayer is indented as it is softer than the tip (a). When the bilayer is no longer able to withstand the loading force, the tip breaks through the whole bilayer and reaches the substrate, producing a single breakthrough step in the F*vs*S curves from which the Fb can be obtained (b). In asymmetric *Lo* domains (Panel B), if no strong coupling occurs, the two leaflets will have different mechanical stability, with a highly ordered phase in the external leaflet and a disordered phase in the proximal leaflet. When the tip reaches the surface of the *Lo* domains, the SM-enriched ordered phase could produce the compression of the disordered DOPC-enriched proximal leaflet as the AFM tip pushes against the top of the more stable *Lo* domains and the loading force increases (a). As the DOPC/Chol leaflet is compressed, a force threshold could be attained at which this leaflet collapses but that it is still not high enough to break through the *Lo* domains. The collapse of the proximal DOPC/Chol leaflet could be detected as a less-defined rupture event in the F*vs*S curves that occurs at lower Fb (b). The loading force continues to increase until it reaches a value high enough to pierce the *Lo* domain present in the remaining external leaflet. Then, the tip jumps through the *Lo* domain and a second rupture event is observed at higher Fb (c).

composition, kinetics of nucleation and domain growth [79]. Nucleation processes proceed as a result of the demixing of the lipid components and respond to compositional changes according to equilibrium thermodynamics. Nevertheless, in the process of domain formation and growth, membrane dynamics plays a central role and, both, the rate of the perturbation that induces the phase transition and the time of response of the membrane are important. So far, most of the information regarding phase separation in ternary lipid systems has come from studies on fixed lipid compositions [80]. Phase segregation in *in situ* generated ternary mixtures—as produced by MβCD-mediated lipid exchange—may take a different path in the phase diagram as the lipid composition will be varying locally and in time. Small variations in the local lipid composition will result in different transient locations in the phase diagram and this in turn will further influence the dynamics of domain formation. As a result, nucleation and growth dynamics may differ from that in phase transitions in fixed lipid mixtures. In addition, the diffusion in supported membranes is slower than in free-standing bilayers and, therefore, the processes that involve lipid and domain motion are expected to be slower, turning membrane dynamics even more relevant [81]. Domains formed in SLBs are therefore likely kinetically trapped non-equilibrium structures.

Phase diagrams for SM-containing systems present regions of gel-fluid coexistence (*Ld* + gel and *Lo* + gel), fluid-fluid coexistence (*Ld* + *Lo*) and three-phase coexistence (*Ld* + *Lo* + gel) [80]. In studies by Veatch et al. on the phase behavior in GUVs of DOPC/16:0SM/Chol, coexisting fluid and solid phases were detected over a wide range of compositions using order-sensitive probes [82]. At 23 °C, gel/Liquid phase coexistence was detected at low Chol levels (0–10%) for 2:1 and 1:1 DOPC/SM mole ratios while at higher SM contents (DOPC/SM 1:2 and 1:4), coexisting gel/Liquid phases appeared up to 20–30% Chol. Notwithstanding, Gel/Liquid phase separation was not observed in any of the previous mixtures when studied at 37 °C, and only *Lo/Ld* phase coexistence was detected at this temperature. Coexisting gel/*Lo/Ld* phases were also detected by AFM microscopy in DOPC/eggSM/Chol (eggSM ~86% 16:0SM) bilayers containing between 44–72% SM and 10–12% Chol when SLBs were cooled from an initially homogenous bilayer at 50 °C to 25 °C [83]. Domain structure was found highly dependent on the cooling rate and the nucleation pathway. The proposition was made then that gel phases containing Chol were difficult to equilibrate sufficiently with a varying balance of lipids and Chol trapped in a non-equilibrium state.

Considering all these, the incorporation of 16:0SM into the outer leaflet of DOPC/Chol bilayers at 24 °C could produce local SM concentrations high enough to induce the formation of gel phases with varying SM/Chol contents. The solid characteristics of the gel phase and the proximity of the rigid substrate may prevent the equilibration with the overall mixture once the domains are formed (at least in our experimental time scales) and, hence, more ordered domains are found coexisting with a *Ld* phase at 24 °C. When SM is incorporated at 37 °C, *Lo* domains may form, even at high SM contents. As both phases are liquid (*Lo/Ld*), they are able to flow and equilibrate to a higher extent even though diffusional processes are slowed down by the substrate.

Finally, it is worth to note that solid supports can alter domain formation and coupling behavior. Studies by Garg et al. in bilayers of PC/SM/Chol produced by Langmuir Blodgett (LB)/Langmuir-Schäfer deposition showed that domain registration—*i.e.*, domains perfectly matched in both leaflets—was only achieved if bilayers were decoupled from the solid support *via* a sufficiently thick hydrophilic polymer layer (~58 Å) [84]. Thus, the degree of interleaflet coupling detected in our asymmetric system could have been influenced by the presence of the

solid support. Tamm and co-workers have used polymer-tethered bilayers to study interleaflet coupling in asymmetric SLBs produced by the LB-vesicle fusion technique [70,72,85]. In their cushioned systems, proximal monolayers composed of lipids typically found in the outer leaflet of plasma membranes that formed *Lo* domains—PC, SM, and Chol—induced the formation of *Lo* phases in several combinations of lipids mimicking the inner leaflet of plasma membranes. Strikingly, *Lo* phases could be induced in complex mixtures but not in simple mixtures of PC/Chol.

4. Conclusion

The asymmetric transbilayer distribution of phospholipids in the plasma membrane of cells confers the two leaflets different potentials to form *raft* domains as next to no sphingolipids are present in the cytoplasmatic leaflet. An important question that has plagued the hypothesis of signal transduction through *rafts* for as long as it has been around is: to what degree are the physical properties in the outer leaflet of the plasma membrane coupled to those of the inner leaflet? Asymmetric model membranes are thus gaining increasing interest nowadays and stand as promising platforms to further elucidate this issue. So far, lipid asymmetry and bilayer physical properties of these systems have been investigated mainly through fluorescent methods, using order-sensitive probes or lipid analogs. In this study, we combined AFM and Force spectroscopy measurements resulting in a detailed nanoscale characterization of asymmetric supported bilayers obtained by lipid substitution that mimic membrane *rafts*. Unraveling the rules that govern domain formation and interleaflet coupling will be facilitated by the experimental strategy outlined here which enables direct measurement of inner and outer leaflet mechanical properties in probe-free bilayers as well as structural characteristics. Furthermore, the lipid exchange method could provide a mechanism to generate asymmetric systems in a biologically relevant way since specific lipids can be incorporated into a preexisting bilayer. The lipid composition of natural membranes is changing continuously due to the incorporation of plasma lipids, membrane recycling, and enzymatic activity, among other cellular processes, and *in situ* modifications in lipid composition can drastically alter membrane properties and protein function. For instance, how the incorporation of omega-3 fatty acids—and other dietary fats—may alter, in *real-time*, the partition behavior of membrane receptors between *Lo* and *Ld* phases can now be explored in a more realistic model system enabling to study the effects of dietary fats on physiological and pathological conditions. How lipid asymmetry could modulate the interaction with extracellular pathogens is another topic widely disregarded that can be studied using these versatile systems.

Finally, the ability to control *Lo*-domains (*rafts*) formation by lipid exchange and its application in live cells is particularly promising for future studies in order to gain deeper insights into the functions of membrane domains *in vivo*.

We hope that these lines of research in asymmetric systems will contribute to a better understanding of membrane biology, eventually supporting the existence of those still hypothetical *lipid rafts*.

Declaration of competing interest

The authors declare that they have no known competing financial interests or personal relationships that could have appeared to influence the work reported in this paper.

Acknowledgements

We thank Arturo Galván-Hernández from Laboratorio de Biofísica of the Instituto de Ciencias Físicas (ICF-UNAM) for technical assistance with the experiments and Mario Raúl Ramos from INIBIOLP for the graphic designs. R.V. thanks the Secretaría de Ciencia y Técnica of Universidad Nacional de La Plata (SeCyT-UNLP) and ICF-UNAM for travel funds. This work was supported by the Agencia Nacional de Promoción Científica y Tecnológica [grant number PICT 881/2018], the Consejo Nacional de Investigaciones Científicas y Técnicas (CONICET) [grant number PIP 948/2017], the Comisión de Investigaciones Científicas de la Provincia de Buenos Aires (CICBA), Universidad Nacional Autónoma de México (UNAM) [DGAPA-PAPIIT-IG100920 and IN209318], and the Consejo Nacional de Ciencia y Tecnología (CONACyT) [grant number PEI-252300]. R.V. is a researcher of UNLP, Argentina. L.B. is a member of the Carrera del Investigador CICBA, Argentina. R.V. and S.M. are members of the Carrera del Investigador of CONICET, Argentina.

References

[1] A.J. Verkleij, R.F. Zwaal, B. Roelofsen, P. Comfurius, D. Kastelijn, L.L. van Deenen, The asymmetric distribution of phospholipids in the human red cell membrane. A combined study using phospholipases and freeze-etch electron microscopy, Biochim. Biophys. Acta 323 (1973) 178–193.
[2] D.L. Daleke, Regulation of transbilayer plasma membrane phospholipid asymmetry, J. Lipid Res. 44 (2003) 233–242.
[3] V.A. Fadok, P.M. Henson, Apoptosis: getting rid of the bodies, Curr. Biol.: CB 8 (1998) R693–R695.
[4] B.R. Lentz, Exposure of platelet membrane phosphatidylserine regulates blood coagulation, Prog. Lipid Res. 42 (2003) 423–438.
[5] M.L. Bader Lange, G. Cenini, M. Piroddi, H.M. Abdul, R. Sultana, F. Galli, M. Memo, D.A. Butterfield, Loss of phospholipid asymmetry and elevated brain apoptotic protein levels in subjects with amnestic mild cognitive impairment and Alzheimer disease, Neurobiol. Dis. 29 (2008) 456–464.
[6] S. Riedl, B. Rinner, M. Asslaber, H. Schaider, S. Walzer, A. Novak, K. Lohner, D. Zweytick, In search of a novel target - phosphatidylserine exposed by non-apoptotic tumor cells and metastases of malignancies with poor treatment efficacy, Biochim. Biophys. Acta 1808 (2011) 2638–2645.
[7] L.A. Bagatolli, J.H. Ipsen, A.C. Simonsen, O.G. Mouritsen, An outlook on organization of lipids in membranes: searching for a realistic connection with the organization of biological membranes, Prog. Lipid Res. 49 (2010) 378–389.
[8] G.L. Nicolson, The Fluid-Mosaic Model of Membrane Structure: still relevant to understanding the structure, function and dynamics of biological membranes after more than 40 years, Biochim. Biophys. Acta 1838 (2014) 1451–1466.
[9] K. Simons, E. Ikonen, Functional rafts in cell membranes, Nature 387 (1997) 569–572.
[10] K. Simons, D. Toomre, Lipid rafts and signal transduction, Nat. Rev. Mol. Cell Biol. 1 (2000) 31–39.
[11] D. Lingwood, H.J. Kaiser, I. Levental, K. Simons, Lipid rafts as functional heterogeneity in cell membranes, Biochem. Soc. Trans. 37 (2009) 955–960.
[12] D. Lingwood, K. Simons, Lipid rafts as a membrane-organizing principle, Science (New York, N.Y.) 327 (2010) 46–50.
[13] D.A. Brown, E. London, Structure and origin of ordered lipid domains in biological membranes, J. Membr. Biol. 164 (1998) 103–114.
[14] L.J. Pike, Rafts defined: a report on the keystone symposium on lipid rafts and cell function, J. Lipid Res. 47 (2006) 1597–1598.
[15] K. Simons, Cell membranes: a subjective perspective, Biochim. Biophys. Acta 1858 (2016) 2569–2572.
[16] J.D. Nickels, S. Chatterjee, C.B. Stanley, S. Qian, X. Cheng, D.A.A. Myles, R.F. Standaert, J.G. Elkins, J. Katsaras, The in vivo structure of biological membranes and evidence for lipid domains, PLoS Biol. 15 (2017) e2002214.
[17] S. Moon, R. Yan, S.J. Kenny, Y. Shyu, L. Xiang, W. Li, K. Xu, Spectrally resolved, functional super-resolution microscopy reveals nanoscale compositional heterogeneity in live-cell membranes, J. Am. Chem. Soc. 139 (2017) 10944–10947.
[18] S.N. Ahmed, D.A. Brown, E. London, On the origin of sphingolipid/cholesterol-rich detergent-insoluble cell membranes: physiological concentrations of cholesterol and sphingolipid induce formation of a detergent-insoluble, liquid-ordered lipid phase in model membranes, Biochemistry 36 (1997) 10944–10953.
[19] C. Dietrich, L.A. Bagatolli, Z.N. Volovyk, N.L. Thompson, M. Levi, K. Jacobson, E. Gratton, Lipid rafts reconstituted in model membranes, Biophys. J. 80 (2001) 1417–1428.
[20] R.M. Sullan, J.K. Li, C. Hao, G.C. Walker, S. Zou, Cholesterol-dependent nanomechanical stability of phase-segregated multicomponent lipid bilayers, Biophys. J. 99 (2010) 507–516.
[21] M.C. Giocondi, D. Yamamoto, E. Lesniewska, P.E. Milhiet, T. Ando, C. Le Grimellec, Surface topography of membrane domains, Biochim. Biophys. Acta 1798 (2010) 703–718.
[22] T.Y. Wang, J.R. Silvius, Cholesterol does not induce segregation of liquid-ordered domains in bilayers modeling the inner leaflet of the plasma membrane, Biophys. J. 81 (2001) 2762–2773.
[23] Q. Lin, E. London, Ordered raft domains induced by outer leaflet sphingomyelin in cholesterol-rich asymmetric vesicles, Biophys. J. 108 (2015) 2212–2222.
[24] R. Takaoka, H. Kurosaki, H. Nakao, K. Ikeda, M. Nakano, Formation of asymmetric vesicles via phospholipase D-mediated transphosphatidylation, Biochim. Biophys. Acta Biomembr. 1860 (2018) 245–249.
[25] M.J. Hope, T.E. Redelmeier, K.F. Wong, W. Rodrigueza, P.R. Cullis, Phospholipid

asymmetry in large unilamellar vesicles induced by transmembrane pH gradients, Biochemistry 28 (1989) 4181–4187.
[26] S. Pautot, B.J. Frisken, D.A. Weitz, Engineering asymmetric vesicles, Proc. Natl. Acad. Sci. U. S. A. 100 (2003) 10718–10721.
[27] W.L. Hwang, M. Chen, B. Cronin, M.A. Holden, H. Bayley, Asymmetric droplet interface bilayers, J. Am. Chem. Soc. 130 (2008) 5878–5879.
[28] H.T. Cheng, E. Megha, London, preparation and properties of asymmetric vesicles that mimic cell membranes: effect upon lipid raft formation and transmembrane helix orientation, J. Biol. Chem. 284 (2009) 6079–6092.
[29] Q. Lin, E. London, Preparation of artificial plasma membrane mimicking vesicles with lipid asymmetry, PLoS One 9 (2014) e87903.
[30] P.C. Hu, S. Li, N. Malmstadt, Microfluidic fabrication of asymmetric giant lipid vesicles, ACS Appl. Mater. Interfaces 3 (2011) 1434–1440.
[31] H.T. Cheng, E. London, Preparation and properties of asymmetric large unilamellar vesicles: interleaflet coupling in asymmetric vesicles is dependent on temperature but not curvature, Biophys. J. 100 (2011) 2671–2678.
[32] S. Chiantia, P. Schwille, A.S. Klymchenko, E. London, Asymmetric GUVs prepared by MbetaCD-mediated lipid exchange: an FCS study, Biophys. J. 100 (2011) L1–L3.
[33] F.A. Heberle, D. Marquardt, M. Doktorova, B. Geier, R.F. Standaert, P. Heftberger, B. Kollmitzer, J.D. Nickels, R.A. Dick, G.W. Feigenson, J. Katsaras, E. London, G. Pabst, Subnanometer structure of an asymmetric model membrane: interleaflet coupling influences domain properties, Langmuir 32 (2016) 5195–5200.
[34] Q. Wang, E. London, Lipid structure and composition control consequences of interleaflet coupling in asymmetric vesicles, Biophys. J. 115 (2018) 664–678.
[35] S. Chiantia, E. London, Acyl chain length and saturation modulate interleaflet coupling in asymmetric bilayers: effects on dynamics and structural order, Biophys. J. 103 (2012) 2311–2319.
[36] C. Wan, V. Kiessling, L.K. Tamm, Coupling of cholesterol-rich lipid phases in asymmetric bilayers, Biochemistry 47 (2008) 2190–2198.
[37] E. London, Membrane structure-function insights from asymmetric lipid vesicles, Acc. Chem. Res. 52 (2019) 2382–2391.
[38] I. Visco, S. Chiantia, P. Schwille, Asymmetric supported lipid bilayer formation via methyl-β-cyclodextrin mediated lipid exchange: influence of asymmetry on lipid dynamics and phase behavior, Langmuir 30 (2014) 7475–7484.
[39] S. Mate, J.V. Busto, A.B. Garcia-Arribas, J. Sot, R. Vazquez, V. Herlax, C. Wolf, L. Bakas, F.M. Goni, N-nervonoylsphingomyelin (c24:1) prevents lateral heterogeneity in cholesterol-containing membranes, Biophys. J. 106 (2014) 2606–2616.
[40] S.M. Mate, R.F. Vazquez, V.S. Herlax, M.A. Daza Millone, M.L. Fanani, B. Maggio, M.E. Vela, L.S. Bakas, Boundary region between coexisting lipid phases as initial binding sites for Escherichia coli alpha-hemolysin: a real-time study, Biochim. Biophys. Acta 1838 (2014) 1832–1841.
[41] M.A. Daza Millone, R.F. Vazquez, S.M. Mate, M.E. Vela, Phase-segregated Membrane Model assessed by a combined SPR-AFM Approach, Colloids Surf. B: Biointerfaces 172 (2018) 423–429.
[42] R.F. Vazquez, M.A. Daza Millone, F.J. Pavinatto, M.L. Fanani, O.N. Oliveira Jr., M.E. Vela, S.M. Mate, Impact of sphingomyelin acyl chain (16:0 vs 24:1) on the interfacial properties of Langmuir monolayers: a PM-IRRAS study, Colloids Surf. B: Biointerfaces 173 (2019) 549–556.
[43] Y.F. Dufrêne, W.R. Barger, J.-B.D. Green, G.U. Lee, Nanometer-scale surface properties of mixed phospholipid monolayers and bilayers, Langmuir 13 (1997) 4779–4784.
[44] S. Garcia-Manyes, F. Sanz, Nanomechanics of lipid bilayers by force spectroscopy with AFM: a perspective, Biochim. Biophys. Acta 1798 (2010) 741–749.
[45] J. Jass, T. Tjarnhage, G. Puu, From liposomes to supported, planar bilayer structures on hydrophilic and hydrophobic surfaces: an atomic force microscopy study, Biophys. J. 79 (2000) 3153–3163.
[46] J.K. Li, R.M. Sullan, S. Zou, Atomic force microscopy force mapping in the study of supported lipid bilayers, Langmuir 27 (2011) 1308–1313.
[47] O. Et-Thakafy, F. Guyomarc'h, C. Lopez, Young modulus of supported lipid membranes containing milk sphingomyelin in the gel, fluid or liquid-ordered phase, determined using AFM force spectroscopy, Biochim. Biophys. Acta Biomembr. 1861 (2019) 1523–1532.
[48] H.A. Rinia, B. de Kruijff, Imaging domains in model membranes with atomic force microscopy, FEBS Lett. 504 (2001) 194–199.
[49] J.C. Lawrence, D.E. Saslowsky, J.M. Edwardson, R.M. Henderson, Real-time analysis of the effects of cholesterol on lipid raft behavior using atomic force microscopy, Biophys. J. 84 (2003) 1827–1832.
[50] T.K. Nyholm, D. Lindroos, B. Westerlund, J.P. Slotte, Construction of a DOPC/PSM/cholesterol phase diagram based on the fluorescence properties of trans-parinaric acid, Langmuir 27 (2011) 8339–8350.
[51] J.H. Ipsen, G. Karlstrom, O.G. Mouritsen, H. Wennerstrom, M.J. Zuckermann, Phase equilibria in the phosphatidylcholine-cholesterol system, Biochim. Biophys. Acta 905 (1987) 162–172.
[52] A. Galvan-Hernandez, N. Kobayashi, J. Hernandez-Cobos, A. Antillon, S. Nakabayashi, I. Ortega-Blake, Morphology and dynamics of domains in ergosterol or cholesterol containing membranes, Biochim. Biophys. Acta Biomembr. 1862 (2020) 183101.
[53] S. Chiantia, J. Ries, N. Kahya, P. Schwille, Combined AFM and two-focus SFCS study of raft-exhibiting model membranes, Chemphyschem Eur. J. Chem. Phys. Phys. Chem. 7 (2006) 2409–2418.
[54] S. Garcia-Manyes, G. Oncins, F. Sanz, Effect of temperature on the nanomechanics of lipid bilayers studied by force spectroscopy, Biophys. J. 89 (2005) 4261–4274.
[55] S. Garcia-Manyes, G. Oncins, F. Sanz, Effect of ion-binding and chemical phospholipid structure on the nanomechanics of lipid bilayers studied by force spectroscopy, Biophys. J. 89 (2005) 1812–1826.
[56] S. Garcia-Manyes, L. Redondo-Morata, G. Oncins, F. Sanz, Nanomechanics of lipid bilayers: heads or tails? J. Am. Chem. Soc. 132 (2010) 12874–12886.
[57] L. Redondo-Morata, M.I. Giannotti, F. Sanz, Structural impact of cations on lipid bilayer models: nanomechanical properties by AFM-force spectroscopy, Mol. Membr. Biol. 31 (2014) 17–28.
[58] R.P. Richter, A. Brisson, Characterization of lipid bilayers and protein assemblies supported on rough surfaces by atomic force microscopy, Langmuir 19 (2003) 1632–1640.
[59] O. Saavedra V, T.F.D. Fernandes, P.-E. Milhiet, L. Costa, Compression, rupture, and puncture of model membranes at the molecular scale, Langmuir 36 (2020) 5709–5716.
[60] L. Redondo-Morata, M.I. Giannotti, F. Sanz, Influence of cholesterol on the phase transition of lipid bilayers: a temperature-controlled force spectroscopy study, Langmuir 28 (2012) 12851–12860.
[61] P.R. Adhyapak, S.V. Panchal, A.V.R. Murthy, Cholesterol induced asymmetry in DOPC bilayers probed by AFM force spectroscopy, Biochim. Biophys. Acta 1860 (2018) 953–959.
[62] S.J. Attwood, Y. Choi, Z. Leonenko, Preparation of DOPC and DPPC supported planar lipid bilayers for atomic force microscopy and atomic force spectroscopy, Int. J. Mol. Sci. 14 (2013) 3514–3539.
[63] T. Maekawa, H. Chin, T. Nyu, T.N. Sut, A.R. Ferhan, T. Hayashi, N.J. Cho, Molecular diffusion and nano-mechanical properties of multi-phase supported lipid bilayers, Phys. Chem. Chem. Phys.: PCCP 21 (2019) 16686–16693.
[64] M.-C. Giocondi, S. Boichot, T. Plénat, C. Le Grimellec, Structural diversity of sphingomyelin microdomains, Ultramicroscopy 100 (2004) 135–143.
[65] S.D. Connell, D.A. Smith, The atomic force microscope as a tool for studying phase separation in lipid membranes, Mol. Membr. Biol. 23 (2006) 17–28.
[66] E.P. Kilsdonk, P.G. Yancey, G.W. Stoudt, F.W. Bangerter, W.J. Johnson, M.C. Phillips, G.H. Rothblat, Cellular cholesterol efflux mediated by cyclodextrins, J. Biol. Chem. 270 (1995) 17250–17256.
[67] R.M. Sullan, J.K. Li, S. Zou, Direct correlation of structures and nanomechanical properties of multicomponent lipid bilayers, Langmuir 25 (2009) 7471–7477.
[68] A. Alessandrini, Heiko M. Seeger, T. Caramaschi, P. Facci, Dynamic force spectroscopy on supported lipid bilayers: effect of temperature and sample preparation, Biophys. J. 103 (2012) 38–47.
[69] M.C. Blosser, A.R. Honerkamp-Smith, T. Han, M. Haataja, S.L. Keller, Transbilayer colocalization of lipid domains explained via measurement of strong coupling parameters, Biophys. J. 109 (2015) 2317–2327.
[70] V. Kiessling, C. Wan, L.K. Tamm, Domain coupling in asymmetric lipid bilayers, Biochim. Biophys. Acta 1788 (2009) 64–71.
[71] B. Eicher, D. Marquardt, F.A. Heberle, I. Letofsky-Papst, G.N. Rechberger, M.S. Appavou, J. Katsaras, G. Pabst, Intrinsic curvature-mediated transbilayer coupling in asymmetric lipid vesicles, Biophys. J. 114 (2018) 146–157.
[72] V. Kiessling, J.M. Crane, L.K. Tamm, Transbilayer effects of raft-like lipid domains in asymmetric planar bilayers measured by single molecule tracking, Biophys. J. 91 (2006) 3313–3326.
[73] R.S. Petruzielo, F.A. Heberle, P. Drazba, J. Katsaras, G.W. Feigenson, Phase behavior and domain size in sphingomyelin-containing lipid bilayers, Biochim. Biophys. Acta 1828 (2013) 1302–1313.
[74] T.K. Nyholm, M. Nylund, J.P. Slotte, A calorimetric study of binary mixtures of dihydrosphingomyelin and sterols, sphingomyelin, or phosphatidylcholine, Biophys. J. 84 (2003) 3138–3146.
[75] R.M. Epand, R.F. Epand, Non-raft forming sphingomyelin-cholesterol mixtures, Chem. Phys. Lipids 132 (2004) 37–46.
[76] N. Jiménez-Rojo, A.B. García-Arribas, J. Sot, A. Alonso, F.M. Goñi, Lipid bilayers containing sphingomyelins and ceramides of varying N-acyl lengths: a glimpse into sphingolipid complexity, Biochim. Biophys. Acta 1838 ((2014) 456–464.
[77] J.P. Slotte, The importance of hydrogen bonding in sphingomyelin's membrane interactions with co-lipids, Biochim. Biophys. Acta 1858 (2016) 304–310.
[78] M.L. Fanani, S. Hartel, R.G. Oliveira, B. Maggio, Bidirectional control of sphingomyelinase activity and surface topography in lipid monolayers, Biophys. J. 83 (2002) 3416–3424.
[79] C.M. Rosetti, A. Mangiarotti, N. Wilke, Sizes of lipid domains: what do we know from artificial lipid membranes? What are the possible shared features with membrane rafts in cells? Biochim. Biophys. Acta Biomembr. 1859 (2017) 789–802.
[80] D. Marsh, Cholesterol-induced fluid membrane domains: a compendium of lipid-raft ternary phase diagrams, Biochim. Biophys. Acta 1788 (2009) 2114–2123.
[81] M. Przybylo, J. Sýkora, J. Humpolíčková, A. Benda, A. Zan, M. Hof, Lipid diffusion in giant unilamellar vesicles is more than 2 times faster than in supported phospholipid bilayers under identical conditions, Langmuir 22 (2006) 9096–9099.
[82] S.L. Veatch, S.L. Keller, Miscibility phase diagrams of giant vesicles containing sphingomyelin, Phys. Rev. Lett. 94 (2005) 148101.
[83] A. Aufderhorst-Roberts, U. Chandra, S.D. Connell, Three-phase coexistence in lipid membranes, Biophys. J. 112 (2017) 313–324.
[84] S. Garg, J. Rühe, K. Lüdtke, R. Jordan, C.A. Naumann, Domain registration in raft-mimicking lipid mixtures studied using polymer-tethered lipid bilayers, Biophys. J. 92 (2007) 1263–1270.
[85] E. Kalb, S. Frey, L.K. Tamm, Formation of supported planar bilayers by fusion of vesicles to supported phospholipid monolayers, Biochim. Biophys. Acta 1103 (1992) 307–316.